Bioactive Materials 4 (2019) 249–255

Contents lists available at ScienceDirect

Bioactive Materials

journal homepage: http://www.keaipublishing.com/biomat

Human mesenchymal stem cell morphology, migration, and differentiation on micro and nano-textured titanium

Emily G. Long[a], Merve Buluk[a], Michelle B. Gallagher[b], Jennifer M. Schneider[b], Justin L. Brown[a,*]

[a] Department of Biomedical Engineering, The Pennsylvania State University, 122 CBEB Building, University Park, PA, 16802, USA
[b] Titan Spine, Inc., Mequon Research Center, 6140 W. Executive Drive, Suite A, Mequon, WI, 53092, USA

ABSTRACT

Orthopedic implants rely on facilitating a robust interaction between the implant material surface and the surrounding bone tissue. Ideally, the interface will encourage osseointegration with the host bone, resulting in strong fixation and implant stability. However, implant failure can occur due to the lack of integration with bone tissue or bacterial infection. The chosen material and surface topography of orthopedic implants are key factors that influence the early events following implantation and may ultimately define the success of a device. Early attachment, rapid migration and improved differentiation of stem cells to osteoblasts are necessary to populate the surface of biomedical implants, potentially preventing biofilm formation and implant-associated infection. This article explores these early stem cell specific events by seeding human mesenchymal stem cells (MSCs) on four clinically relevant materials: polyether ether ketone (PEEK), Ti6Al4V (smooth Ti), macro-micro rough Ti6Al4V (Endoskeleton®), and macro-micro-nano rough Ti6Al4V (nanoLOCK®). The results demonstrate the incorporation of a hierarchical macro-micro-nano roughness on titanium produces a stellate morphology typical of mature osteoblasts/osteocytes, rapid and random migration, and improved osteogenic differentiation in seeded MSCs. Literature suggests rapid coverage of a surface by stem cells coupled with stimulation of bone differentiation minimizes the opportunity for biofilm formation while increasing the rate of device integration with the surrounding bone tissue.

1. Introduction

Orthopedic disease and injuries often require the repair or replacement of a joint or damaged/diseased bone tissue with a bone graft, bone graft substitute or biomedical implant. The interface between an orthopedic implant and the surrounding bone tissue is key to the ultimate success of the implant. Ideally, this interface will encourage osseointegration with the host bone, resulting in strong fixation and implant stability. However, implant failure can occur due to the lack of integration with bone tissue or bacterial infection. The chosen material and surface topography of orthopedic implants are key factors that influence the early events following implantation and may ultimately define the success of a device.

Upon implantation, bacteria compete with somatic and progenitor cells to populate the surface, resulting in either biofilm formation or healthy tissue. The phrase “race for the surface”, initially coined by Gristina in 1987, describes the competition between microbial adhesion and tissue integration at the implant surface [1–3]. The goal of this “race for the surface” is to have tissue specific stem cells occupy the implanted surface and minimize the ability of bacteria to form biofilms, which obstruct cellular functions and can negatively affect the formation of healthy tissue. Additionally, bacterial biofilms are more resistant to antibacterial agents as compared to their planktonic counterparts and also resist natural host defense mechanisms [4]. Thus, the ability for stem cells to adhere, spread and migrate may mitigate the likelihood of biofilm formation and biomaterial associated infections (BAI) [5–7]. The prevention of BAIs is especially important for orthopedic devices as aseptic loosening and infection remain the leading causes of implant failure [8].

The ideal implant interface will encourage rapid migration, proliferation and differentiation of stem cells to osteoblasts and eventually osteocytes, producing an osteoid matrix that ultimately mineralizes and creates a cohesive interface between the implant and surrounding tissue. The local stem cell population that contributes to the formation of bone tissue are mesenchymal stem cells (MSCs) [9]. These MSCs exist in both periosteal and endosteal membranes lining the exterior and interior of existing bones in addition to being found in many other connective tissues, such as, adipose tissue [10]. Complicating the ability to form bone tissue is the multilineage potential of MSCs. MSCs can readily differentiate to adipose tissue, bone tissue, cartilage and other connective tissue, and muscle tissue [9,11]. Successful orthopedic implants should direct the differentiation of MSCs towards only bone tissue.

The presentation of the implant surface is key to the events from cell adhesion through differentiation. Both the chemistry of the chosen material and surface topography affect the response of MSCs post

Peer review under responsibility of KeAi Communications Co., Ltd.
* Corresponding author.
E-mail address: justinbrown@psu.edu (J.L. Brown).

https://doi.org/10.1016/j.bioactmat.2019.08.001
Received 29 March 2019; Received in revised form 24 July 2019; Accepted 26 August 2019
Available online 19 September 2019

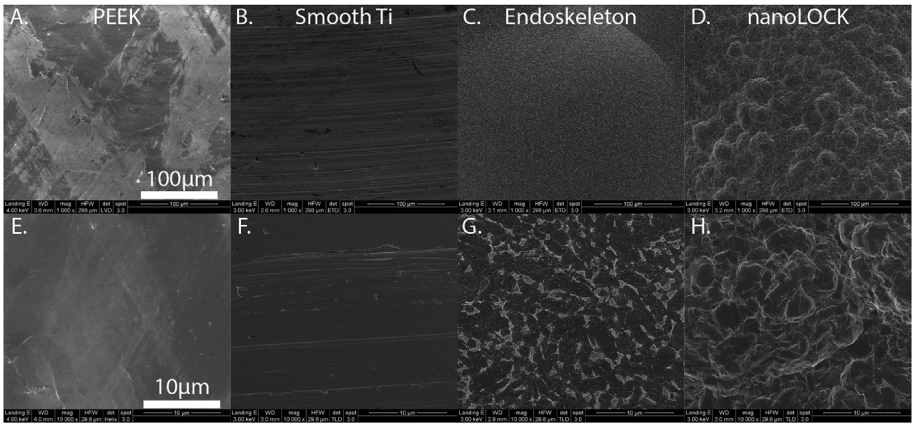

Fig. 1. Surfaces were imaged with SEM to demonstrate the unique nanostructures present on the nanoLOCK® surface relative to Endoskeleton®. A. – D. are 1,000X images for PEEK, Smooth Ti, Endoskeleton® and nanoLOCK® respectively. E. – H. are 10,000X images for PEEK, Smooth Ti, Endoskeleton® and nanoLOCK® respectively.

implantation [12–15]. Specific to this article is an examination of how micro and hierarchical nano/microtextured surfaces influence early MSC response [16]. The interaction with an MSC and a surface is carried out through multiple protein complexes and organelles, which range in size from 10's of nanometers up to a few microns. Modulating these protein complexes and organelles can be accomplished through varying surface features presenting similar characteristic dimensions [17–21]. One key protein complex involved in MSC fate is the focal adhesion, which is a cluster of integrins attaching the cell to a surface and numerous associated intracellular proteins capable of both structural and biochemical activity [22,23]. Unique nanostructures can alter this integrin signaling leading to cytoskeletal reorganization and morphology changes, and subsequently alter differentiation [24,25]. Furthermore, we have previously detailed how nanostructures can affect and direct the differentiation of MSCs towards bone tissue [17–20]. Specifically, what we have found is that hierarchical nano/microtextured surfaces can increase intracellular contractility and directing MSC differentiation to bone [18]. Based on the ability of changes in surface features at the micro- and nanoscale to influence a wide range of cellular activities including: adhesion, spreading, morphology, proliferation and differentiation; we postulate that the presentation of a textured surface influencing cell adhesion, migration and differentiation of MSCs may be a non-toxic and localized option to minimize the opprotunity for bacterial adhesion and biofilm formation, decreasing the chance of BAI.

Two clinically relevant materials utilized in orthopedic applications are polyether ether ketone (PEEK) and the titanium alloy Ti_6Al_4V, (Ti). We have previously demonstrated the material choice and topography of the surface have the ability to regulate the early attachment, migration and differentiation of human mesenchymal stem cells (MSCs) [13,16,26]. In that work, Ti surfaces exhibiting macro-micro roughness resulted in improved cell spreading, random migration and increased differentiation towards an osteoblastic lineage when compared with smooth topographies, both Ti and PEEK [16]. Specifically, the macro-micro texture on the Ti led to early cuboidal and stellate morphologies indicative of osteogenic differentiation, while smooth topographies resulted in elongated spindle-shaped cells at 24 h, typical of a fibroblastic tissue.

In this article, we expand on the previous study by introducing a surface with specifically engineered micro- and nano-topography. This study will examine: the rate of morphology change, rate of adhesion to a surface, velocity and directionality of migration, and differentiation of MSCs. The rate of morphology change is an indicator of adhesion, spreading and possibly differentiation. Further, rapid random migration is advantageous to establish a cohesive layer of MSCs on a surface. Finally, differentiation of MSCs to osteoblasts may be assessed through the early osteoblast marker, alkaline phosphatase (ALP) and the maturing osteoblast marker, osterix (OSX). We hypothesize that a unique combination of micro and nanotexture on Ti will improve the rate of morphology change to steady state and enhance the rate of MSC differentiation to bone tissue.

2. Materials and methods

2.1. Substrate preparation

Substrates were 15-mm diameter disks machined from titanium alloy (Ti6Al4V ELI per ASTM F136) and PEEK (per ASTM F2026) to create relatively smooth surfaces (Titan Spine, Inc., Mequon, WI). To create the roughened surface textures, titanium disks were treated with a proprietary acid etch process creating a macro and micro texture, herein referred to as Endoskeleton®. Some of the disks were additionally treated with a proprietary process that imposes a nano texture onto the roughened titanium surfaces, herein referred to as nanoLOCK®. All disks were sterilized by immersion in 70% ethanol for 30 min and rinsed with 1x phosphate-buffered saline (PBS) prior to use.

To characterize the surface features, a disk from each unique surface was imaged with scanning electron microscopy (SEM). SEM imaging was carried out on a FEI Nova NanoSEM 630 SEM (ThermoFisher, Waltham, MA, USA). Representative images were acquired on each of the 4 unique surfaces at 1,000X and 10,000X. These images are presented in Fig. 1.

2.2. Cell culture

Human mesenchymal stem cells (MSCs) were obtained from Lonza and maintained in a basal media composed of: αMEM (ThermoFisher, Waltham, MA, USA) with 10% fetal bovine serum (Atlanta Biologicals, Atlanta, GA, USA) and 1% penicillin/streptomycin (ThermoFisher, Waltham, MA, USA). MSCs were seeded on each of the surfaces at 1000 cells/cm^2 for evaluating morphology and migration, and 10,000 cells/cm^2 for assaying early differentiation.

2.3. Morphology and cell adehsion

To evaluate morphology MSCs were stained with the DiI derivative, DiR (ThermoFisher, Waltham, MA, USA) to fluorescently label the cell membrane. The staining was carried out through addition of 0.5% DiR in basal media and subsequent incubation for 30 min in a humidified incubator. The stained MSCs were trypsinized and plated on each of the four surfaces, which were imaged at 2, 6, 24 and 72hrs. An average of 20 MSCs per timepoint per surface were analyzed to determine a representative morphology. The images were thresholded and processed with the 'Analyze Particles' function within ImageJ (NIH) to identify perimeter (P), area (A), long axis length (L) and short axis length (S). Aspect ratio, circularity and roundness were calculated as follows:

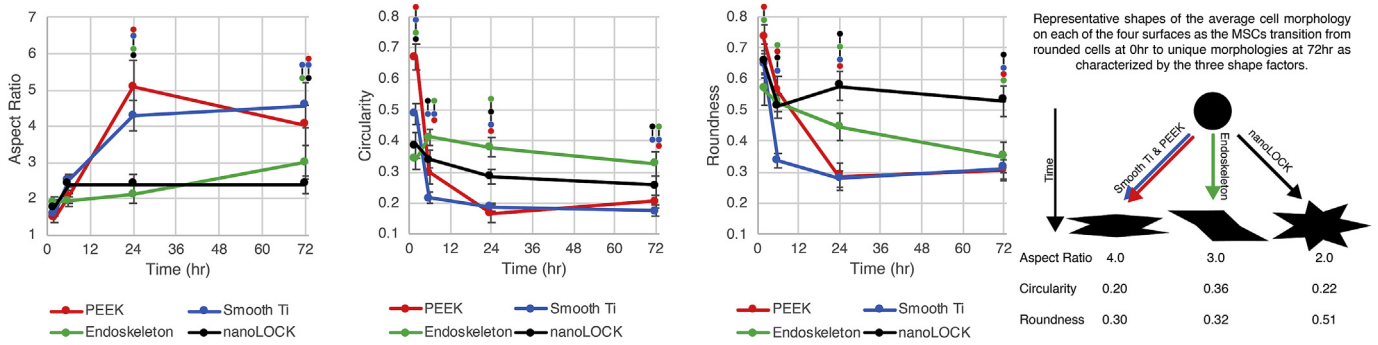

Fig. 2. MSC morphology was determined on each of the four unique surfaces by measuring Aspect Ratio, A., Circularity, B., and Roundness, C. Significance ($p < 0.05$) between surfaces at a single time point are represented by bars between circles matched to the color corresponding to the surface. Furthermore, to demonstrate how these three shape factors relate to cell shapes observed, D., provides representative shapes near the average measured shape factors at 72 h for all four surfaces.

$$Aspect\ Ratio = \frac{L}{S},\quad Circularity = \frac{4\pi A}{P^2},\quad Roundness = \frac{4A}{\pi L^2}$$

Furthermore, to evaluate MSCs attached to a surface, MSCs were stained with DiR following the protocol above and were imaged at 2, 12 and 24hrs. The number of MSCs adhered was recorded for 5 unique regions on each surface to determine the kinetics of MSC adhesion.

Qualitative immunofluorescence images were obtained of representative MSCs at 24hrs on each of the four surfaces through first fixation of the samples in 3.7% paraformaldehyde (Sigma-Aldrich, St. Louis, MO, USA) followed by blocking and permeabilization in 0.1% Triton X-100 (Sigma-Aldrich, St. Louis, MO, USA) with 2% bovine serum albumin (VWR, Radnor, PA, USA) and probing with CF568 phalloidin (Biotium, Freemont, CA, USA) or Atto490LS phalloidin for PEEK specifically (Sigma-Aldrich, St. Louis, MO, USA), DAPI (ThermoFisher, Waltham, MA, USA), and a primary antibody to the protein vinculin (Sigma-Aldrich, St. Louis, MO, USA) followed by a secondary antibody conjugated to Dylight 488 (ThermoFisher, Waltham, MA, USA) or Q dot 800 for PEEK specifically (ThermoFisher, Waltham, MA, USA) [16,20,27,28]. Z-projected 3D deconvolved slices of the immunostained MSCs were overlaid with a reflected differential interference contrast (DIC) image in grayscale of the surface obtained through a z-projected 3D inverse filtered stack to produce the resulting images of the MSCs on each surface.

2.4. Migration

To evaluate migration velocity and directionality, MSCs were first loaded with quantum dots using the Qtracker 705 Cell Labeling kit (ThermoFisher, Waltham, MA, USA) following the manufacturers protocol. The labelled cells were trypsinized and seeded on each of the four surfaces. Migrating MSCs were imaged at 10X on a heated microscope stage every 10min from 6hr–16hr post seeding, an average of 8 MSCs were tracked on each surface. The acquired time-lapse images were processed with ImageJ (NIH) to determine velocities in addition to displacement. The displacements were used to calculate directionality as follows:

$$Directionality = \frac{end - to - end\ distance}{total\ distance}$$

2.5. Differentiation

MSCs were seeded on all four surfaces and maintained in basal media supplemented with 3 mM β-glycerophosphate (Sigma-Aldrich, St. Louis, MO, USA) and 50 μg/mL ascorbic acid (Sigma-Aldrich, St. Louis, MO, USA). At 3d and 10d samples were lysed in 200 μL of mammalian protein extraction reagent, M-PER, (ThermoFisher, Waltham, MA, USA) and transferred to −80C for storage. DNA was measured with a Quant-iT PicoGreen assay (ThermoFisher, Waltham, MA, USA), alkaline phosphatase, ALP, was measured with a p-nitrophenolphosphate assay (ThermoFisher, Waltham, MA, USA), and osterix, OSX, was measured with an OSX/SP-7 ELISA (LifeSpan Biosciences, Seattle, WA, USA). All assays were used by following the manufacturers protocols, with a sample volume of 5 μL.

2.6. Statistics

n = 4 was used for all quantitative assays. Morphology was measured for an average of 21 cells per sample per time point, an n = 5 unique regions per surface were used to quantify cell adhesion, and migration velocity and directionality were calculated for an average of 8 cells per sample. One-way ANOVAs with Tukey post hoc tests were used to determine significant differences in MSC morphology, migration, directionality and differentiation markers, ALP and OSX, which were first normalized to the DNA content per sample.

3. Results and discussion

3.1. Morphology

MSC morphology was examined quantitatively at 2, 6, 24 and 72hrs post seeding on smooth Ti, a microtextured Ti (Endoskeleton®), a hierarchical nano/microtextured Ti (nanoLOCK®), and polyether ether ketone (PEEK). Furthermore, a qualitative examination was carried out through immunostaining at 24hr. Fig. 2 presents the quantitative analysis of MSC morphology. Fig. 2 examines cell shape through three unique shape indicators: aspect ratio, circularity and roundness. An unspread, rounded cell would present an aspect ratio of 1.0, circularity of 1.0 and roundness of 1.0. Fig. 2A demonstrates the aspect ratio shift on all four surfaces. At the 2hr time point all four surfaces demonstrated aspect ratios under 2.0 with no significance between the groups. Examining temporal changes in aspect ratio, between the 2hr and 6hr time points, PEEK, smooth Ti and nanoLOCK® all demonstrated significant increases in aspect ratio. From 6hrs onward through 72hr, nanoLOCK® did not demonstrate any significant changes in aspect ratio, whereas all three other surfaces demonstrated significant shifts between the 6hr and 72hr time points. Examining changes between groups, both the nanoLOCK® and Endoskeleton® surfaces were significantly lower in aspect ratio than the smooth Ti and PEEK at 24hrs, and nanoLOCK® was again significantly lower at 72 h than both, but Endoskeleton® was only lower than smooth Ti.

Fig. 2B demonstrates the shift in circularity values over time on all four surfaces. Circularity significantly decreased on smooth Ti and PEEK from 2hr to 6hr; however, neither Endoskeleton® nor nanoLOCK® demonstrated significant changes from 2hr to 6hr. Furthermore, only PEEK demonstrated a significant change in circularity between 6hr and

24hr, suggesting a lag in reaching the steady state cell morphology. Examining changes in circularity between groups, Endoskeleton® presented the highest circularity from 6hr onward, and was significantly higher circularity than smooth Ti and PEEK at 6, 24 and 72hrs and nanoLOCK® at 24hr. Furthermore, PEEK and smooth Ti demonstrated the lowest circularity from 6hr onward.

Finally, Fig. 2C presents the shift in roundness over time on all four surfaces. All four surfaces demonstrated a sharp decrease in roundness from 2hr to 6hrs, followed by a leveling off for all surfaces but Endoskeleton®. Smooth Ti demonstrated significantly lower roundness at 6hr than all other surfaces, whereas, nanoLOCK® demonstrated significantly higher roundness at 24hr and 72hr as compared to all other surfaces. Taken together the morphology results indicate a general trend towards an elongated morphology for smooth Ti and PEEK, characterized by high aspect ratios, low circularity and low roundness. The low aspect ratio, high circularity and moderate roundness on Endoskeleton® indicate a trend towards cuboidal morphologies and finally the low aspect ratio, moderate circularity and high roundness indicate a trend towards stellate morphologies on nanoLOCK®.

Quantitative analysis of MSC adhesion on all four surfaces at 2, 12 and 24hr, Fig. 3., reveals the MSCs adhered to nanoLOCK® rapidly compared with the other surfaces. All titanium surfaces, nanoLOCK®, Endoskeleton® and smooth Ti, demonstrated higher than 20% of MSCs adhered by 2hr, whereas, PEEK only demonstrated 10% of MSCs adhered by 2hr. At 12 h peak adhesion occurred on nanoLOCK® with a density equivalent to 90% the initial seeding density. Endoskeleton® also demonstrated a plateau by 12hr, however, only approximately 50% of seeded cells were attached. Adhesion to the smooth Ti occurred at a slower ratel, but 50% of seeded MSCs ultimately adhered to the surface by 24hr. PEEK also exhibited a plateau at 12 h, but only 30% of the seeded cells attached by 24hrs.

Qualitative morphology at 24hrs follows the expected trends uncovered in the quantitative morphology, and is presented in Fig. 4 and Supplemental Figure 1. Notably, both PEEK and smooth Ti demonstrated elongated or spindle shaped MSCs. Endoskeleton® presented cuboidal MSCs and nanoLOCK® presented stellate MSCs. Evaluating the presence of focal adhesions as indicated by the focal adhesion protein vinculin, stained green, it is clear that both Endoskeleton® and nanoLOCK® present peripheral focal adhesions, smooth Ti presents very large elongated focal adhesions and PEEK qualitatively presents the fewest focal adhesions of the four. Together the qualitative morphology follows the quantitative assessment and focal adhesion formation suggests cell adhesion is poor on PEEK.

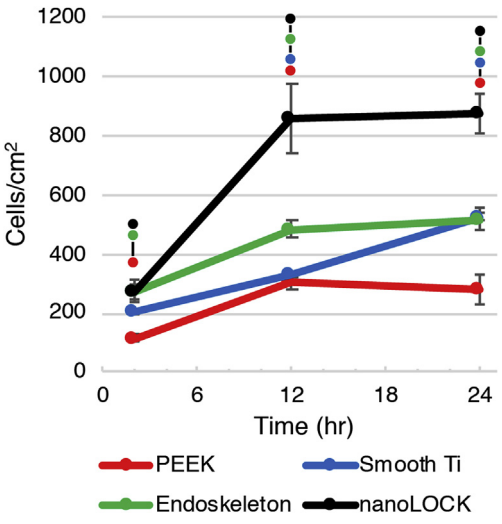

Fig. 3. MSC adhesion kinetics were assessed over the course of 24 h by counting the number of cells attached to each surface at 2hr, 12hr, and 24hr. Significance ($p < 0.05$) between surfaces at a single time point are represented by bars between circles matched to the color corresponding to the surface.

3.2. Migration

MSC migration velocity and directionality were quantified on each of the four surfaces from 6 to 16hr post seeding. Migration velocities varied dramatically on the four surfaces, Fig. 5A., with PEEK demonstrating the slowest average velocity of 32.9 μm/hr followed by Endoskeleton® at 39.8 μm/hr and smooth Ti and nanoLOCK® presenting the highest average velocities of 55.6 μm/hr and 56.3 μm/hr, respectively. Velocity was significantly higher on smooth Ti as compared to both Endoskeleton® and PEEK, similarly, nanoLOCK® was significantly higher than PEEK. Directionality of the migrating MSCs was significantly higher on smooth Ti as compared to all other surfaces, Fig. 5B.

Rose plots were generated from velocities, Fig. 6, and demonstrates an anomaly in the quantified directionalities presented in Fig. 5B. The rose plots for Endoskeleton® and nanoLOCK® both demonstrate MSCs moving in multiple directions, which is expected based on the low quantified directionalities. Similarly, smooth Ti also mimics the measured directionality by demonstrating most migration along a single axis and in a single direction; however, PEEK demonstrates MSCs clearly moving along a single axis, but in both directions. This opposite and bidirectional movement of MSCs on PEEK is why the quantified directionality is low and does not indicate random migration as observed on Endoskeleton® and nanoLOCK®.

3.3. Differentiation

Finally, MSC differentiation was assessed at 3d and 10d post seeding on all four surfaces, Fig. 7. The first marker assessed was the early bone marker ALP, which is expressed primarily by preosteoblasts and expression decreases in osteoblasts and is not expressed at all in terminally differentiated osteocytes. Fig. 7A demonstrates ALP expression by MSCs on the four surfaces normalized to DNA concentration on each surface. At 3d post seeding, nanoLOCK® had significantly higher ALP expression than all other surfaces. In contrast, at 10d nanoLOCK® had less ALP than all other surfaces and was the only of the four to not demonstrate a significant increase between 3d and 10d. At 10d smooth Ti demonstrated the highest expression of ALP, which was found to be significantly higher than either Endoskeleton® or nanoLOCK®. Furthermore, ALP expression on PEEK at 10d was significantly higher than nanoLOCK®. Next, the maturing osteoblast marker, OSX, was examined and normalized to DNA concentration, Fig. 7B. OSX is expressed by preosteoblasts transitioning to osteoblasts. At 3d post seeding, OSX expression was low on all surfaces. At 10d, both Endoskeleton® and nanoLOCK® demonstrated significantly higher OSX expression as compared to 3d. Furthermore, expression of OSX was significantly different between both Endoskeleton® and nanoLOCK® from all other surfaces, with nanoLOCK® demonstrating the highest expression of OSX as compared to all other surfaces. All differentiation markers are normalized to the DNA concentration of each sample, which is presented in Supplemental Figure 2. Analysis of both osteogenic markers indicate the cells on the nanoLOCK® surface were the most differentiated, followed by Endoskeleton®, smooth Ti, and PEEK.

3.4. Discussion

The influence of surface chemistry and topography on osteoblast differentiation is well established in literature. Previous work on the early response of MSCs demonstrated that material choice and macro/micro-scale topography can regulate the early attachment, migration and differentiation of hMSCs [13,16,26]. Specifically, the macro-micro texture on titanium led to early cuboidal and stellate morphologies indicative of osteogenic differentiation, while smooth topographies resulted in elongated spindle-shaped cells, typical of a fibroblastic

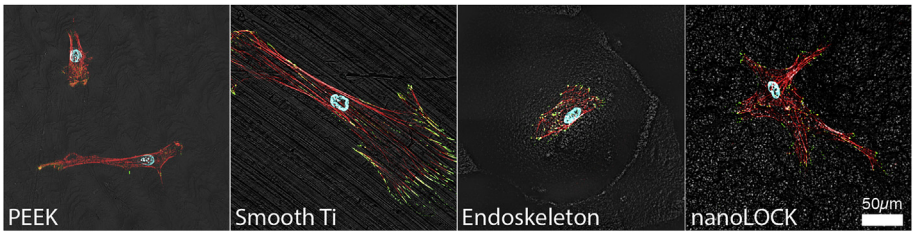

Fig. 4. Representative 40X immunofluorescence images of MSCs on each surface at 24hrs actin stress fibers (red), the focal adhesion protein vinculin (green), and the nuclei (blue).

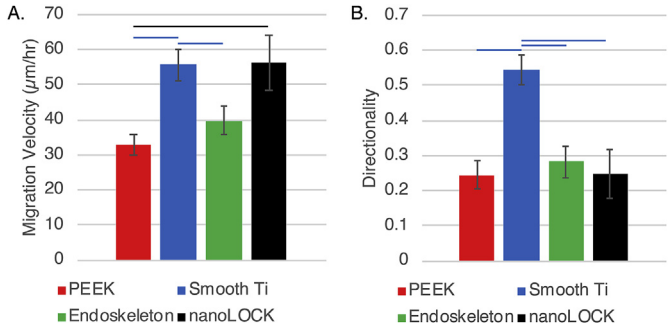

Fig. 5. MSC migration velocity, A., and directionality, B., were examined on each of the four surfaces. Significance ($p < 0.05$) is represented by bars that are matched to the color corresponding to the surface.

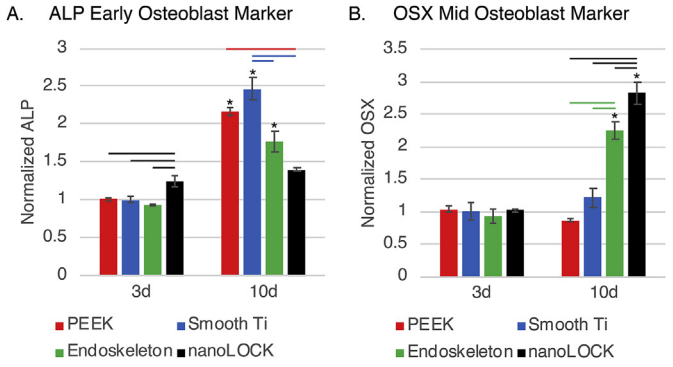

Fig. 7. Assessment of hMSC differentiation through the early marker alkaline phosphatase (ALP), A., and mid marker osterix (OSX), B., at 3 and 10 days. Significance ($p < 0.05$) is demonstrated between surfaces at the same time by bars, and on the same surface across the time points by *'s.

tissue. In conjunction, differentiation outcomes illustrated increased levels of ALP and OSX on the texture titanium indicating greater movement towards the osteogenic lineage compared with the smooth topographies. The goals of the present study were to expand on the previous study by introducing a surface with specifically engineered micro- and nano-topography to evaluate the influence of the combined topography on early response of MSCs and its correlation with long-term osteoblastic differentiation.

The success of an orthopedic implant/graft depends on the ability of the surface of the implant/graft to stimulate rapid adhesion, migration and differentiation of MSCs to bone tissue. As an MSC attaches and spreads on a surface the morphology of the MSC shifts from a sphere that transitions to a range of potential morphologies, such as: elongated spindle shaped MSCs; cuboidal or polygonal shaped MSCs; or MSCs demonstrating multiple large processes, referred to as stellate morphologies. There is currently some debate as to whether morphology correlates with lineage commitment of the MSCs [29,30]. However, the research demonstrating no clear correlation focused on spreading of MSCs with round versus elongated shapes only, not the unique cuboidal or stellate morphologies of more mature osteoblasts/osteocytes [29]. We examined temporal changes in aspect ratio, circularity and roundness to assess the early MSC morphology changes in response to PEEK, smooth Ti, Endoskeleton® and nanoLOCK® surfaces. Based on a high initial circularity and increased lag in reaching a steady-state in all three metrics of morphology, it is clear that MSCs on PEEK were the slowest to adapt to the surface and reach a steady-state morphology. This delay may be in part due to poor surface adhesion of the cells as indicated by the lower quantity of focal adhesions observed at 24hrs. The eventual steady-state morphology of MSCs on PEEK was long spindle shaped cells as evident by the high aspect ratio coupled with low circularity and roundness at 72 h. In contrast, MSCs on all the Ti alloy surfaces rapidly reached a steady-state morphology, however, these morphologies were quite dissimilar and appeared dependent on surface topography. MSCs on smooth Ti reached an elongated spindle shaped morphology similar to PEEK, however at a faster rate and with stronger surface adhesion as indicated by the quantity of focal adhesions. MSCs on Endoskeleton® demonstrated polygonal and cuboidal morphologies as evident by a low aspect ratio, high circularity, and moderate roundness. Finally, MSCs on nanoLOCK® demonstrated stellate morphologies with numerous large processes in multiple directions characterized by low aspect ratio, moderate circularity but high roundness. Comparing the observed morphologies to expected morphologies of the target tissue, bone typically demonstrates both cuboidal and stellate morphologies with mature cells demonstrating longer cell processes [16,31,32]. In contrast, the spindle morphologies observed on both smooth Ti and PEEK are typical of fibroblasts and other connective tissues, such as, tendon and ligament [33,34].

The "race for the surface" relies on rapid adhesion and occupation of an implant by MSCs [1,2]. This requires cells to attach, and migrate randomly and rapidly to evenly distribute across the available area [35]. The adhesion kinetics demonstrate nanoLOCK® promotes rapid adhesion of MSCs, followed by Endoskeleton®, smooth Ti, and PEEK.

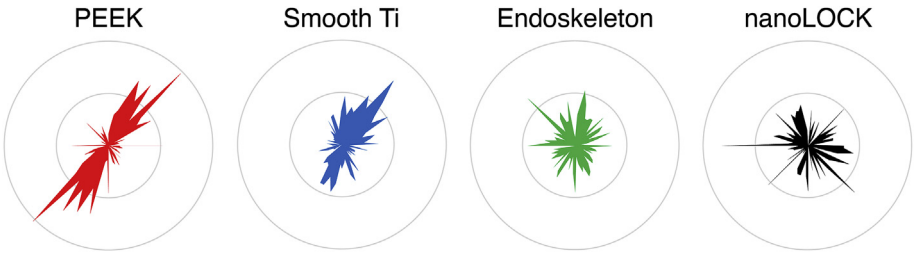

Fig. 6. Circular histograms demonstrating the migration direction of all cells measured on each surface, demonstrating that Endoskeleton® and nanoLOCK® did indeed present true random migration, whereas, PEEK demonstrated migration in two opposite directions.

Furthermore, the migration data demonstrates that cells on both Endoskeleton® and nanoLOCK® surfaces achieved the target of random migration, but nanoLOCK® demonstrated a much higher velocity. In contrast cells on both smooth Ti and PEEK demonstrated migration along a single axis, potentially a result of contact guidance along the ridges created by machining [36,37]. These differences in migration velocity and direction between rough and smooth topographies are consistent with the original study. Together this data suggests the hierarchical nano/microstructure present on nanoLOCK® surfaces was advantageous for generating the rapid and random migration necessary for bone tissue integration with the implant.

Finally, osteogenic markers were evaluated for correlation with the early morphology results. An implant needs to stimulate the formation of *de novo* bone tissue to ensure cohesive integration with the surrounding bone tissue. This integration ensures the implant behaves as a single unit with existing tissue. The two markers assayed evaluate early to mid-osteoblast differentiation. nanoLOCK® in particular did not show any measurable change in ALP expression between 3d and 10d, however the 3d expression was significantly higher than the other three surfaces. This suggests that peak ALP expression on nanoLOCK® surfaces may have occurred between the 3d and 10d time points. Evaluating the other surfaces, Endoskeleton® also presented only a modest increase in ALP, whereas both smooth Ti and PEEK presented strong increases in ALP. Typical *in vitro* differentiation of MSCs on tissue culture polystyrene results in peak ALP activity around 14d post seeding, however, biomaterials and nanostructures tend to accelerate this response [38,39]. To further elucidate the rates of differentiation on the four surfaces the second marker, OSX, proves valuable because it typically demonstrates a peak in expression later than ALP, approximately 2–3 weeks both *in vitro* and *in vivo* during fracture healing [40–42]. OSX expression on nanoLOCK® was significantly elevated at 10d as compared to all other surfaces, suggesting that MSCs were rapidly differentiating to osteoblasts. Furthermore, Endoskeleton® presented a moderate level of OSX at 10d, which when coupled with the moderate increase in ALP suggests MSC differentiation on Endoskeleton® was rapid but lagged the differentiation on nanoLOCK®. Finally, both smooth Ti and PEEK presented low levels of OSX at 10d, which when coupled with high ALP expression suggests that MSCs on both of these surfaces are differentiating to osteoblasts at the slowest rates observed. Together this data suggests MSC differentiation to osteoblasts on nanoLOCK® was dramatically improved as compared to all other surfaces, and MSC differentiation to osteoblasts on PEEK was the lowest observed on all four surfaces.

4. Conclusions

Together the data presented above validates our two initial hypotheses. Notably, incorporating a specifically engineered micro- and nano-roughness on Ti6Al4V improves the rate of adhesion and velocity of migrating MSCs in addition to the increasing the rate at which the MSCs differentiate to osteoblasts. Furthermore, this improved differentiation correlates with a rapid adoption of a stellate morphology by the MSCs on the nanoLOCK® surfaces, suggesting this morphology may be an appropriate predictor of substrate success. These results support the combined macro-micro-nano topography of the nanoLOCK® surface as being a substantial improvement over other topographies for osseointegration as demonstrated through rapid random migration necessary to populate a surface with stem cells, the evolution of a morphology typical of mature osteoblasts/osteocytes, and a rapid progression through the early and mid-osteogenic differentiation markers, ALP and OSX respectively. Rapid surface adhesion and spreading by mesenchymal stem cells coupled with stimulation of bone differentiation potentially minimizes the opportunity for bacteria colonization, thus winning the “race to the surface”, and increases the rate of device integration with surrounding bone tissue.

Conflicts of interest

Michelle B. Gallagher and Jennifer M. Schneider are employed by Titan Spine, Inc.

Acknowledgements

This work was funded through a sponsored research agreement between the Pennsylvania State University and Titan Spine, Inc, Mequon, WI.

Appendix A. Supplementary data

Supplementary data to this article can be found online at https://doi.org/10.1016/j.bioactmat.2019.08.001.

References

[1] A. Gristina, P. Naylor, Q. Myrvik, Infections from biomaterials and implants: a race for the surface, Med. Prog. Technol. 14 (1987) 205–224.
[2] A.G. Gristina, Biomaterial-centered infection: microbial adhesion versus tissue integration, Science 237 (1987) 1588–1595, https://doi.org/10.1126/science.3629258.
[3] G. Subbiahdoss, R. Kuijer, D.W. Grijpma, H.C. van der Mei, H.J. Busscher, Microbial biofilm growth vs. tissue integration: “The race for the surface” experimentally studied, Acta Biomater. 5 (2009) 1399–1404, https://doi.org/10.1016/j.actbio.2008.12.011.
[4] P.S. Stewart, J.W. Costerton, Antibiotic resistance of bacteria in biofilms. Lancet 358: 135–138, Lancet 358 (2001) 135–138, https://doi.org/10.1016/S0140-6736(01)05321-1.
[5] K. Anselme, P. Davidson, A.M. Popa, M. Giazzon, M. Liley, L. Ploux, The interaction of cells and bacteria with surfaces structured at the nanometre scale, Acta Biomater. 6 (2010) 3824–3846, https://doi.org/10.1016/j.actbio.2010.04.001.
[6] M. Bächle, R.J. Kohal, A systematic review of the influence of different titanium surfaces on proliferation, differentiation and protein synthesis of osteoblast-like MG63 cells, Clin. Oral Implant. Res. 15 (2004) 683–692, https://doi.org/10.1111/j.1600-0501.2004.01054.x.
[7] K. Anselme, M.B.A. biomaterialia, Topography effects of pure titanium substrates on human osteoblast long-term adhesion, Acta Biomater. 1 (2005) 211–222, https://doi.org/10.1016/j.actbio.2004.11.009.
[8] J.W. Costerton, Biofilm theory can guide the treatment of device-related orthopaedic infections, Clin. Orthop. Relat. Res. 437 (2005) 7.
[9] M. Krampera, G. Pizzolo, G. Aprili, M. Franchini, Mesenchymal stem cells for bone, cartilage, tendon and skeletal muscle repair, Bone 39 (2006) 678–683, https://doi.org/10.1016/j.bone.2006.04.020.
[10] M.N. Knight, K.D. Hankenson, Mesenchymal stem cells in bone regeneration, Adv. Wound Care 2 (2013) 306–316, https://doi.org/10.1089/wound.2012.0420.
[11] M.F. Pittenger, A.M. Mackay, S.C. Beck, R.K. Jaiswal, R. Douglas, J.D. Mosca, et al., Multilineage potential of adult human mesenchymal stem cells, Science 284 (1999) 143–147, https://doi.org/10.1126/science.284.5411.143.
[12] A. Joy, D.M. Cohen, A. Luk, E. Anim-Danso, C. Chen, J. Kohn, Control of surface chemistry, substrate stiffness, and cell function in a novel terpolymer methacrylate library, Langmuir 27 (2011) 1891–1899, https://doi.org/10.1021/la103722m.
[13] R. Olivares-Navarrete, S.L. Hyzy, D.L. Hutton, C.P. Erdman, M. Wieland, B.D. Boyan, et al., Direct and indirect effects of microstructured titanium substrates on the induction of mesenchymal stem cell differentiation towards the osteoblast lineage, Biomaterials 31 (2010) 2728–2735, https://doi.org/10.1016/j.biomaterials.2009.12.029.
[14] R. Olivares-Navarrete, S.L. Hyzy, R.A. Gittens I, J.M. Schneider, D.A. Haithcock, P.F. Ullrich, et al., Rough titanium alloys regulate osteoblast production of angiogenic factors, Spine J. 13 (2013) 1563–1570, https://doi.org/10.1016/j.spinee.2013.03.047.
[15] R. Olivares-Navarrete, R.A. Gittens, J.M. Schneider, S.L. Hyzy, D.A. Haithcock, P.F. Ullrich, et al., Osteoblasts exhibit a more differentiated phenotype and increased bone morphogenetic protein production on titanium alloy substrates than on poly-ether-ether-ketone, Spine J. 12 (2012) 265–272, https://doi.org/10.1016/j.spinee.2012.02.002.
[16] B.L. Banik, T.R. Riley, C.J. Platt, J.L. Brown, Human mesenchymal stem cell morphology and migration on microtextured titanium, Front. Bioeng. Biotechnol. 4 (2016) 41, https://doi.org/10.3389/fbioe.2016.00041.
[17] A.M. Higgins, B.L. Banik, J.L. Brown, Geometry sensing through POR1 regulates Rac 1 activity controlling early osteoblast differentiation in response to nanofiber diameter, Integr. Biol. 7 (2015) 229–236, https://doi.org/10.1039/C4IB00225C.
[18] T. Ozdemir, L.-C. Xu, C. Siedlecki, J.L. Brown, Substrate curvature sensing through Myosin IIa upregulates early osteogenesis, Integr. Biol. 5 (2013) 1407–1416, https://doi.org/10.1039/c3ib40068a.
[19] T. Ozdemir, D.T. Bowers, X. Zhan, D. Ghosh, J.L. Brown, Identification of key signaling pathways orchestrating substrate topography directed osteogenic differentiation through high-throughput siRNA screening, Sci. Rep. 9 (2019) 1001, https://doi.org/10.1038/s41598-018-37554-y.

[20] D. Jaiswal, J.L. Brown, Nanofiber diameter-dependent MAPK activity in osteoblasts, J. Biomed. Mater. Res. 100 (2012) 2921–2928, https://doi.org/10.1002/jbm.a.34234.
[21] V. Vogel, M. Sheetz, Local force and geometry sensing regulate cell functions, Nat. Rev. Mol. Cell Biol. 7 (2006) 265–275, https://doi.org/10.1038/nrm1890.
[22] R. Zaidel-Bar, B. Geiger, The switchable integrin adhesome, J. Cell Sci. 123 (2010) 1385–1388, https://doi.org/10.1242/jcs.066183.
[23] E. Kritikou, Networks: the complexity of adhesion, Nat. Rev. Mol. Cell Biol. 8 (2007) 674–675, https://doi.org/10.1038/nrm2237.
[24] K.A. Kilian, B. Bugarija, B.T. Lahn, M. Mrksich, Geometric cues for directing the differentiation of mesenchymal stem cells, Proc. Natl. Acad. Sci. 107 (2010) 4872–4877, https://doi.org/10.1073/pnas.0903269107.
[25] A.J. Engler, S. Sen, H.L. Sweeney, D.E. Discher, Matrix elasticity directs stem cell lineage specification, Cell 126 (2006) 677–689, https://doi.org/10.1016/j.cell.2006.06.044.
[26] R.A. Gittens, R. Olivares-Navarrete, T. McLachlan, Y. Cai, S.L. Hyzy, J.M. Schneider, et al., Differential responses of osteoblast lineage cells to nanotopographically-modified, microroughened titanium–aluminum–vanadium alloy surfaces, Biomaterials 33 (2012) 8986–8994, https://doi.org/10.1016/j.biomaterials.2012.08.059.
[27] P. Fattahi, J.T. Dover, J.L. Brown, 3D near-field electrospinning of biomaterial microfibers with potential for blended microfiber-cell-loaded gel composite structures, Adv. Healthc. Mater. 260 (2017) 1700456, https://doi.org/10.1002/adhm.201700456.
[28] B.L. Banik, G.S. Lewis, J.L. Brown, Multiscale poly-(ε-caprolactone) scaffold mimicking non-linearity in tendon tissue mechanics, Regen. Eng. Transl. Med. (2016) 1–9, https://doi.org/10.1007/s40883-016-0008-5.
[29] A.C. Jimenez-Vergara, R. Zurita, A. Jones, P. Diaz-Rodriguez, X. Qu, K.L. Kusima, et al., Refined assessment of the impact of cell shape on human mesenchymal stem cell differentiation in 3D contexts, Acta Biomater. (2019), https://doi.org/10.1016/j.actbio.2019.01.052.
[30] M. Guvendiren, J.A. Burdick, The control of stem cell morphology and differentiation by hydrogel surface wrinkles, Biomaterials 31 (2010) 6511–6518, https://doi.org/10.1016/j.biomaterials.2010.05.037.
[31] T.A. Franz-Odendaal, B.K. Hall, P.E. Witten, Buried alive: how osteoblasts become osteocytes, Dev. Dynam. 235 (2006) 176–190, https://doi.org/10.1002/dvdy.20603.
[32] M.L. Knothe Tate, "Whither flows the fluid in bone?" an osteocyte's perspective, J. Biomech. 36 (2003) 1409–1424.
[33] M. Dalby, M. Riehle, D. Sutherland, H. Agheli, E. al, Morphological and microarray analysis of human fibroblasts cultured on nanocolumns produced by colloidal lithography, Eur. Cells Mater. 9 (2005) 1–8.
[34] Z. Yin, X. Chen, J.L. Chen, W.L. Shen, T.M.H. Nguyen, L. Gao, et al., The regulation of tendon stem cell differentiation by the alignment of nanofibers, Biomaterials 31 (2010) 2163–2175, https://doi.org/10.1016/j.biomaterials.2009.11.083.
[35] M.H. Gail, C.W. Boone, The locomotion of mouse fibroblasts in tissue culture, Biophys. J. (1970), https://doi.org/10.1016/S0142-9612(99)00205-7.
[36] P. Clark, P. Connolly, A.S. Curtis, J.A. Dow, C.D. Wilkinson, Topographical control of cell behaviour: II. Multiple grooved substrata, Development 108 (1990) 635–644.
[37] A.D. Doyle, F.W. Wang, K. Matsumoto, K.M. Yamada, One-dimensional topography underlies three-dimensional fibrillar cell migration, J. Cell Biol. 184 (2009) 481–490, https://doi.org/10.1083/jcb.200810041.
[38] A. Shafiee, E. Seyedjafari, M. Soleimani, N. Ahmadbeigi, P. Dinarvand, N. Ghaemi, A comparison between osteogenic differentiation of human unrestricted somatic stem cells and mesenchymal stem cells from bone marrow and adipose tissue, Biotechnol. Lett. 33 (2011) 1257–1264, https://doi.org/10.1007/s10529-011-0541-8.
[39] J.L. Brown, M.S. Peach, L.S. Nair, S.G. Kumbar, C.T. Laurencin, Composite scaffolds: bridging nanofiber and microsphere architectures to improve bioactivity of mechanically competent constructs, J. Biomed. Mater. Res. 95 (2010) 1150–1158, https://doi.org/10.1002/jbm.a.32934.
[40] A. Ulsamer, M.J. Ortuño, S. Ruiz, A.R.G. Susperregui, N. Osses, J.L. Rosa, et al., BMP-2 induces Osterix expression through up-regulation of Dlx5 and its phosphorylation by p38, J. Biol. Chem. 283 (2008) 3816–3826, https://doi.org/10.1074/jbc.M704724200.
[41] L.A. Kaback, Y Soung Do, A. Naik, N. Smith, E.M. Schwarz, R.J. O'Keefe, et al., Osterix/Sp7 regulates mesenchymal stem cell mediated endochondral ossification, J. Cell. Physiol. 214 (2008) 173–182, https://doi.org/10.1002/jcp.21176.
[42] E. Ragni, T. Montemurro, E. Montelatici, C. Lavazza, M. Vigano, P. Rebulla, et al., Differential microRNA signature of human mesenchymal stem cells from different sources reveals an "environmental-niche memory" for bone marrow stem cells, Exp. Cell Res. 319 (2013) 1562–1574, https://doi.org/10.1016/j.yexcr.2013.04.002.